Cohesive-frictional model for bond and splitting action of prestressing wire

J. C. Gálvez[1,*,†], J. M. Benítez[2], M. J. Casati[3], B. S. Tork[4] and D. A. Cendón[5]

[1]*Departamento de Ingeniería Civil: Construcción, E.T.S. de Ingenieros de Caminos, Canales y Puertos Universidad Politécnica de Madrid, 28040 Madrid, Spain*
[2]*Departamento de Vehículos Aeroespaciales, E.T.S. de Ingenieros Aeronáuticos, Universidad Politécnica de Madrid, 28040 Madrid, Spain*
[3]*Departamento de Vehículos Aeroespaciales, E.U. Ingeniería Técnica Aeronáutica, Universidad Politécnica de Madrid, 28040 Madrid, Spain*
[4]*Ain Shams University, El Cairo, Egypt*
[5]*Departamento de Ciencia de Materiales, Universidad Politécnica de Madrid, E.T.S. Ingenieros de Caminos, Canales y Puertos C/Profesor Aranguren s/n, 28040 Madrid, Spain*

SUMMARY

This paper presents a numerical procedure for bond between indented wires and concrete, and the coupled splitting process of the surrounding concrete. The bond model is an interface, non-associative, plasticity model. It is coupled with a cohesive fracture model for concrete to take into account the splitting of such concrete. Bond between steel and concrete is fundamental for the transmission of stresses between both materials in precast prestressed concrete. Indented wires are used to improve the bond in these structural elements. The radial component of the prestressing force, increased by Poisson's effect, may split the surrounding concrete, decreasing the wire confinement and diminishing the bonding. The combined action of the bond and the splitting is studied with the proposed model. The results of the numerical model are compared with the results of a series of tests, such as those which showed splitting induced by the bond between wire and concrete. Tests with different steel indentation depths were performed. The numerical procedure accurately reproduces the experimental records and improves knowledge of this complex process.

KEY WORDS: concrete; prestressed concrete; bond-splitting; fracture; modelling; finite element

1. INTRODUCTION

Bond action of prestressed wire generates forces that tend to split the surrounding concrete. The pioneering work of Tepfers [1] provides a useful model for bar reinforced concrete (see Figure 1). Such a model has been extensively used since its proposal. Bond-splitting action of ribbed bars has been examined by many researchers, such as Tepfers and Olsson [2], Cairns and Jones [3, 4], Gambarova and Rosati [5], Abrishami and Mitchell [6], Ogura *et al.* [7], Jendele and Cervenka [8] and Malvar [9], among others. Less attention has been devoted to prestressed concrete elements. In this field, bond stress versus slip curves has been studied: den Uijl [10], Abrishami and Mitchell [11], Tassios and Bonataki [12] and Report FIB [13], with a certain amount of attention being paid to the splitting action of the radial stresses and loss of confinement induced by

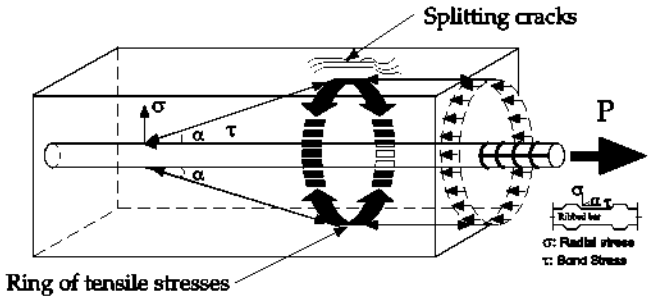

Figure 1. Bond behaviour of deformed bars, radial component of the bond stresses balanced by tensile stresses in the uncracked ring of concrete [1].

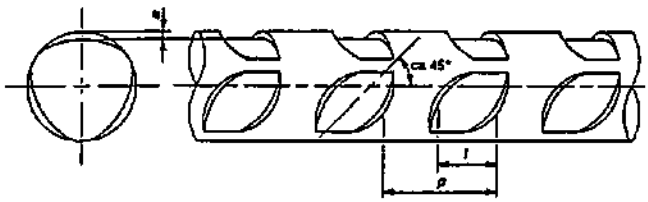

Figure 2. Geometry of the indentations of the wire [22].

longitudinal cracking. Several researchers have studied experimentally the analogy between the splitting action of the reinforcement in bond and the pressure of liquid in a pipe or sleeve [14]. Two-dimensional plane strain models have been proposed, which are focussed on concrete fracture with no relationship between steel sliding and radial stresses being included, with even Poisson's effect being omitted [15, 16]. There is no model for bond and splitting action of prestressing indented wire.

This paper presents a numerical procedure to simulate the bond between indented wire and concrete, and the possible coupled splitting process of the surrounding concrete. An interface, non-associative, plasticity model for bond between indented wire and concrete is proposed. The bond model is conceptually based on the proposal of Cox and Hermann [17–19] for ribbed steel bars by means of an interface with a non-associative plasticity model. Our bond model is performed for prestressed concrete and only includes parameters that can be experimentally measured. This bond model is coupled with a fracture model for concrete to take into account the splitting of the concrete, an aspect which is not included in the pioneering work of Cox and Hermann [17–19].

The mechanisms that contribute to bond between prestressed steel and surrounding concrete are chemical adhesion, friction and mechanical interlocking between wire indentations and concrete [20]. The geometry of the surface of the wire is extremely important for bond [21] and is standardized [22]. Figure 2 shows the indention geometry of the wire, and Table I shows the dimensions of the indentations.

It is worth noting that Hoyer's effect is present at the ends of the prestressed concrete element (see Figure 3). Such an effect is directly related with Poisson's effect and magnifies the mechanical action generated by the indentations of the wire, increasing the tension ring on these local zones [23]. These combined aspects are beneficial for bond, though they may be harmful if concrete splits, dropping confinement and diminishing the bond [10, 11, 23, 24].

The numerical model is validated with the experimental results of two series of bond-splitting tests. The two main influencing parameters on bond splitting are studied: the depth of the wire indentation and the thickness of the concrete cover of the wire. One of the series is performed with large specimens [23, 25], in which the bond stress along the wire is not uniform, and the other with short specimens [26], in which a uniform bond stress along the wire can be expected.

Table I. Specified indentation dimensions, according to UNE 36094 [22].

	Dimensions of indentations			
	Depth a (mm $\times 10^{-2}$)			
Nominal wire diameter (mm)	Type 1	Type 2	Length l(mm)	Spacing p (mm)
3	2–6		3.5±0.5	5.5±0.5
4	3–7	5–9		
5	4–8	6–10		
6	5–10	8–13	5.0±0.5	8.0±0.5
⩾7	6–12	10–20		

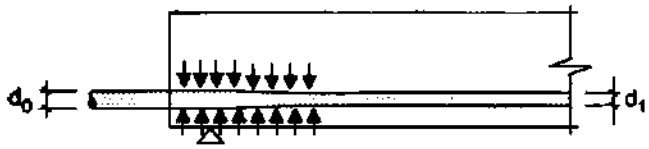

Figure 3. Sketch of the Hoyer's effect.

In this paper the authors seek to emphasize that with this new approach, combining cohesive fracture of concrete and bond between wire and concrete, it is possible to analyse the influence of the parameters affecting bond in the splitting failure of the concrete. It is acknowledged that further work should be carried out to extend this modelling to the majority of the prestressed concrete structural elements.

The model was developed and experimentally evaluated with prestressed single wires. The cross section of a wire has a well-defined perimeter in contact with concrete and there is no helicoidal rotation when it slips (this effect affects three- and seven-wire strands). Extension of the model to strands by adopting the suitable parameters does not present significant problems, especially with regard to the equivalent perimeter in contact with concrete.

In comparison with previous bond models, such as the Cox and Hermann model [17–19], the proposed numerical procedure accomplishes both the bond modelling and the splitting of the surrounding concrete, taking into account the loss of confinement of the wire or strand. This combined effect, bond and splitting, is fundamental to study the longitudinal cracking problems in linear precast prestressed concrete beams, joists and hollow core slabs. As far as the authors know, there is currently no model that accomplishes both effects, bond and splitting.

Whereas the following section examines the numerical modelling, Section 3 presents an overview of the experimental programme. Model validation is then presented in Section 4. Discussion is presented in Section 5. Finally, the conclusions obtained from the model are presented in Section 6.

2. NUMERICAL MODELLING OF BOND SPLITTING

2.1. Problem posing

Two processes require modelling: (1) the possible splitting of the concrete induced by the radial pressure of the wire; (2) the bond in the interface between concrete and steel. The two processes are related. In this work the model of the splitting concrete failure is based on the cohesive crack approach [27], and that of the bond on a plasticity formulation [23, 25]. Figure 4 shows a sketch of both the processes to be modelled.

2.2. The cohesive crack model

The cohesive crack model is generally accepted as a realistic simplification of the fracture of quasi-brittle materials. Such a model was proposed by Hillerborg *et al.* [27] in the late 1970s,

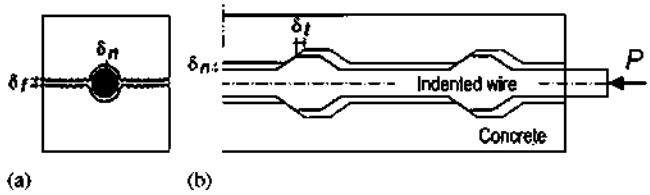

Figure 4. Numerical problem processes: (a) longitudinal cracking of concrete (splitting) and (b) bond-slip behaviour of the interface between wire and concrete.

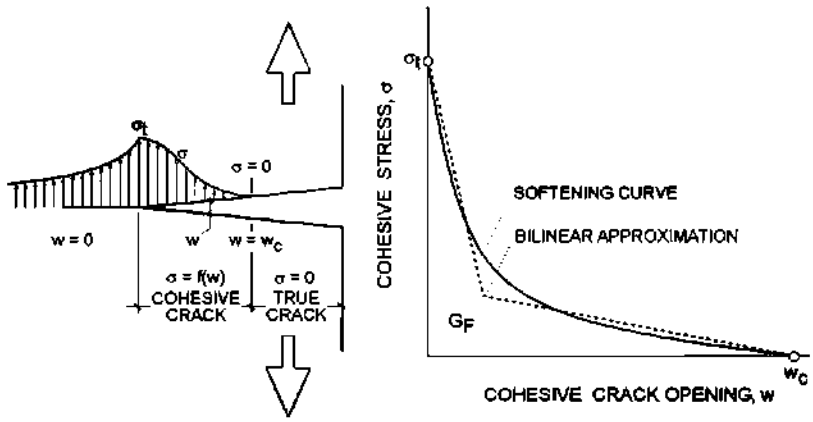

Figure 5. Cohesive crack, softening function and notation for mode I fracture of quasi-brittle materials.

and has been successful in the analysis of the fracture of concrete and concrete-like materials since its proposal. The softening function, $\sigma = f(w)$, is the main ingredient of the cohesive crack model. This function, a material property, relates the stress σ acting across the crack faces to the corresponding crack opening w (see Figure 5). In mode I opening, the stress transferred, σ, is normal to the crack faces. A detailed study of this model has been published by Bazant and Planas [28].

Two properties of the softening curve are most important: the tensile strength, f_t, and the cohesive fracture energy, G_F. The tensile strength being the stress at which the crack is created and starts to open ($f(0) = f_t$). The cohesive fracture energy, G_F, also called *specific fracture energy*, is the external energy supply required to create a full break unit surface area of a cohesive crack, and coincides with the area under the softening function.

The tensile strength and the specific fracture energy are material properties and may be experimentally measured in accordance with ASTM C 496 [29] and RILEM 50-FMC [30], respectively.

2.3. *The bond model*

The interface between concrete and steel transmits normal and tangential stresses and shows *dilatancy*. The bar-scale approach, according to Cox's terminology [18, 25], is adopted, with the wire–concrete interface being idealized in terms of two simplifications: (1) uniform distribution of the bond stress for a unit surface element (Figure 6(a)) and (2) idealized deformation of the concrete in the bond zone (Figure 6(b)).

2.3.1. Yield surface for bonding. The relative displacement between the wire and concrete at the interface is vectorial in nature. We denote it as **u**, with normal and shear components denoted as u_n and u_t, i.e.

$$\mathbf{u} = u_n \vec{n} + u_t \vec{t} \tag{1}$$

where $\vec{n}$ and $\vec{t}$ are the unit vectors, respectively, normal and tangential to the surface of the wire.

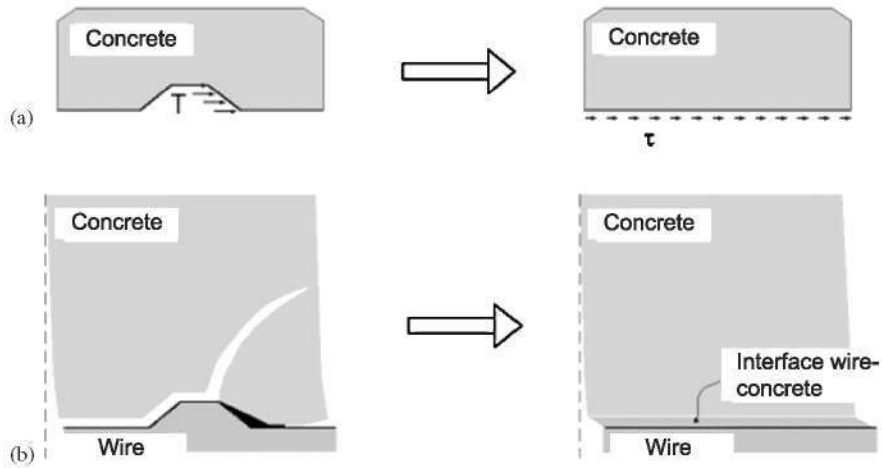

Figure 6. Sketch of the idealized interface between wire and concrete for a unit surface element: (a) uniform distribution of the bond stress and (b) deformation of the concrete in the bond zone.

Likewise, the stress transferred on the interface between the concrete and the wire is also vectorial, and is characterized by the vector $\mathbf{t}$ acting on the interface; with normal and tangential components denoted as σ and τ, i.e.

$$\mathbf{t}=\sigma\vec{n}+\tau\vec{t} \tag{2}$$

In this work, elastoplastic formulation is adopted, in which the interface displacement is split into its elastic and inelastic parts

$$\mathbf{u}=\mathbf{u}^e+\mathbf{u}^i; \quad \dot{\mathbf{u}}=\dot{\mathbf{u}}^e+\dot{\mathbf{u}}^i \tag{3}$$

For the inelastic behaviour, it is assumed that the inelastic displacement can progress when the yield surface $F(t)=0$ is reached, similar to the yield surface in classical plasticity. The following hyperbolic expression has been assumed by the authors [31, 32]:

$$F(\mathbf{t})=\tau^2-\tan\phi_{\mathrm{f}}(f_{\mathrm{t}}-\sigma)[2c-\tan\phi_{\mathrm{f}}(f_{\mathrm{t}}+\sigma)] \tag{4}$$

where ϕ_{f} is the friction angle between the wire and concrete, c the cohesion (bond strength without interface normal stress), and f_{t} the tensile strength in the normal direction to the interface. These values are *instantaneous* values and depend on loading history through the effective inelastic crack displacement u^{ieff}, defined by the conditions

$$\dot{u}^{\mathrm{ieff}}=\|\dot{\mathbf{u}}^i\|=((\dot{u}_{\mathrm{n}}^i)^2+(\dot{u}_{\mathrm{t}}^i)^2)^{0.5} \tag{5}$$

$$u^{\mathrm{ieff}}=\int \dot{u}^{\mathrm{ieff}}\,\mathrm{d}t \tag{6}$$

In this work it is assumed that the friction angle ϕ_{f} is constant, whereas the instantaneous tensile strength f_{t} and cohesion c depend on u^{ieff} bilinearly as depicted in Figure 7.

Following the analogy with the cohesive model, the area under the softening curve for f_{t} may be interpreted as the specific fracture energy $G_{\mathrm{F}}^{\mathrm{I}}$ for mode I, and the area under the softening curve for the cohesion c (which also has dimensions of energy per unit area) as the mode IIa (shear under normal confinement) specific fracture energy $G_{\mathrm{F}}^{\mathrm{IIa}}$ [33]. For the particular case of bond, this

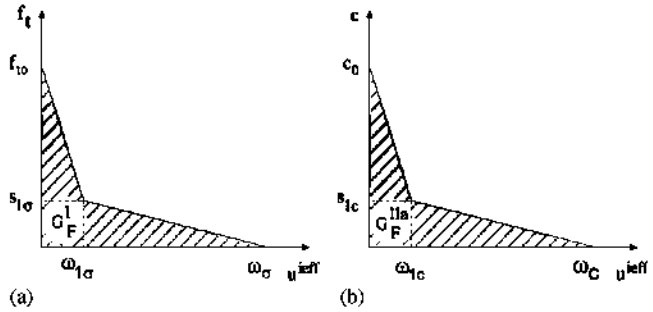

Figure 7. Softening curves for the strength of the interface between wire and concrete: (a) normal direction (tensile strength) and (b) tangential direction (bond strength).

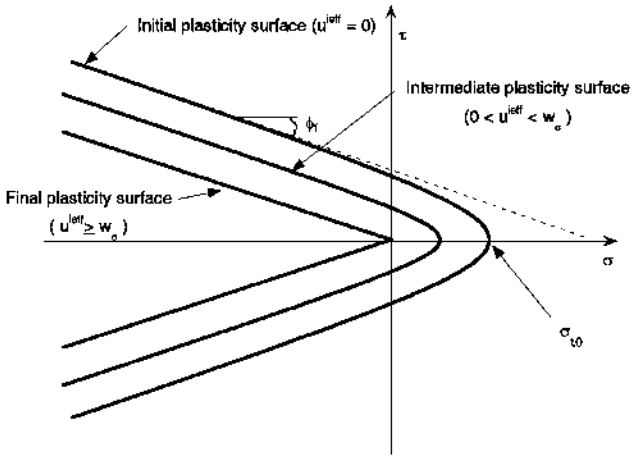

Figure 8. Plasticity surface and evolution.

one may be measured by means of a pull-out test under high confinement. The following values for ω_c and ω_s in the softening curves (see Figure 7) are adopted

$$\omega_c = \frac{2G_F^{IIa} - (s_{1c} + c_0)\omega_{1c}}{s_{1c}} \tag{7}$$

$$\omega_\sigma = \frac{2G_F^{I} - (s_{1\sigma} + f_{t0})\omega_{1\sigma}}{s_{1\sigma}} \tag{8}$$

Figure 8 shows the plasticity surface for bonding in the interface, and its evolution with the parameter u^{ieff}. Note that for each state of damage, the hyperbolic plasticity surface has two branches and only the branch extending towards negative values of σ is physically acceptable. Furthermore, it should also be noted that for fully damaged interface (complete loss of tensile strength and cohesion), the plasticity surface degenerates into a Coulomb friction surface with friction coefficient $\mu = \tan\phi_f$.

2.3.2. Flow rule and dilatancy. Owing to the dilatant behaviour of the wire–steel interface (the indentation of the wire opens the surrounding concrete when slips), non-associative plasticity has been adopted. Then, the evolution of the inelastic displacements in the interface zone is specified by means of the flow rule, given by

$$\dot{\mathbf{u}}^i = \dot{\lambda}\frac{\partial Q(\mathbf{t})}{\partial \mathbf{t}} = \dot{\lambda}\mathbf{b} \tag{9}$$

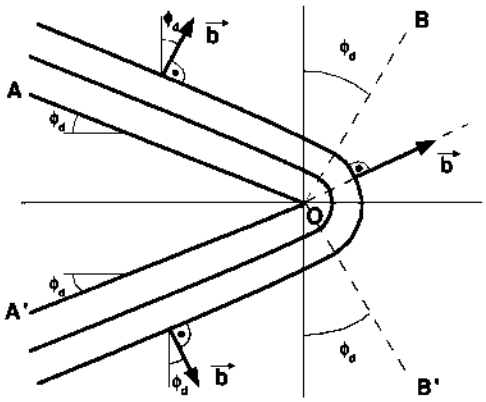

Figure 9. Return direction to the plasticity surface of the inelastic corrector.

where $Q(\mathbf{t})$ is the plastic potential, $\mathbf{b}$ is the normal to the plastic potential surface and $\dot{\lambda}$ is a non-negative plastic multiplier. The adopted plastic potential is

$$Q(\mathbf{t}) = (\sigma \tan \phi_d) - \tau^2 = 0$$

where σ and τ are the normal and tangential components of the stress, ϕ_{d} is the dilatancy angle. The dilatancy angle ϕ_{d} is also defined

$$\tan \phi_{\mathrm{d}} = \frac{\dot{u}_{\mathrm{n}}^{i}}{\dot{u}_{\mathrm{t}}^{i}} \tag{10}$$

where $\dot{u}_{\mathrm{n}}^{i}$ and $\dot{u}_{\mathrm{t}}^{i}$ are the incremental inelastic displacements in the normal and tangential directions to the interface, respectively. ϕ_{d} coincides with the angle formed by the potential surface and the negative part of the σ axis (see Figure 9).

The dilatancy angle is also assumed to depend on the damage level through u^{ieff}. Following References [31, 33], a linear curve has been adopted:

$$\phi_{\mathrm{d}} = \begin{cases} \phi_{\mathrm{d0}} \left(1 - \dfrac{u^{\mathrm{ieff}}}{u_{\mathrm{cd}}} \right) & \forall u^{\mathrm{ieff}} < u_{\mathrm{cd}} \\ 0 & \forall u^{\mathrm{ieff}} \geqslant u_{\mathrm{cd}} \end{cases} \tag{11}$$

where ϕ_{d0} is the initial value of the dilatancy angle and u_{cd} is the critical inelastic crack displacement after which the interface ceases to exhibit the dilatancy effect.

When traction stress σ is predominant over the tangential stress τ (the right part of OBB'), the direction normal to the plastic potential ($Q = \mathrm{cte}$) is not defined. Consequently, in this case the return direction to the origin of stresses is adopted, which divides the stresses space into two parts, as shown in Figure 9. It should be pointed out that this is a non-associative plasticity approach, where normal directions to cracking surface and plastic potential are different.

2.3.3. Incorporation into a finite element code. An interface element was developed to incorporate the bond model in the finite element code ABAQUS©. Figure 10 shows the interface finite element, for 2D and 3D analysis. The cohesive model for simulation of the radial cracks was included by means of non-linear springs. Details regarding the finite element implementation are found in [25]. A global arc length algorithm (spherical arc length) was adopted for the computational procedure and no special difficulties were found in achieving a convergent solution.

To simplify the computations, the bulk behaviour of the material outside of the crack and the interface was assumed to be linear-elastic and isotropic, although this approximation could have been relaxed if necessary.

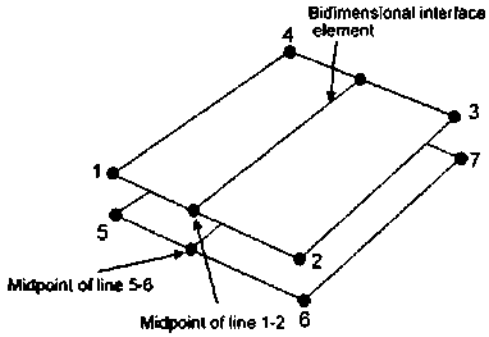

Figure 10. Sketch of the interface finite element: red line for 2D simplified interface finite element.

3. OVERVIEW OF THE EXPERIMENTAL PROGRAMME

The experimental programme was designed to study the combined action of the bond and the splitting in prestressed concrete during the prestressing force release.

Pull-out and push-in tests with short embedment length are often used to study the bond characteristics of the reinforcing tendons [13]. This is due to the fact that bond stresses are not uniformly distributed along the embedment length. As a result, the difference between the maximum and the average value increases with the bonded length. To obtain a unique bond stress-slip relation the embedment length should be as short as possible. For other reasons, such as scatter of results due to inhomogeneity of concrete and indentation spacing, a practical length of three to five times the tendon diameter is often used [13]. The differences between pull-out and push-in tests have been studied for strand [10, 11].

In this work the push-in type test is adopted. Such a test is more suitable for studying the bond and splitting action of the wire, given that it incorporates the radial transverse expansion of the wire and implicitly includes its influence in bond and in the radial compressive stress at the interface. Two series of *push-in* tests have been adopted: specimens with *large* and *short* embedded length of the prestressed wire.

A test with large embedment length was performed to analyse the observed coupled bond-splitting process in joists (Figure 11). Figure 11(b) shows the influence of the Hoyer's effect at the end of the joists. Figure 12 shows a sketch of the joist with the geometry and dimensions adopted for the specimens in the experimental analysis. For the sake of simplicity, specimens with only one wire and a rectangular shaped cross section were performed.

A test with short embedment length was performed as a push-in standard test [13]. Both tests were performed with the same material and are complementary for a strong validation of the numerical model.

3.1. Materials

The specimens were manufactured with concrete, composed of Portland cement, siliceous sand and siliceous crushed coarse aggregates of 6mm maximum size. Table II shows the composition of the mixture. Table III shows the mechanical properties of the concrete at the test age.

EN-10138 Y 1770 C 4 I [34] wires were selected. Table III shows the mechanical properties of the wires, with the nominal diameter being 4 mm. Wires with three indentation depths (shallow, medium and deep) were used. These are shown in Table IV.

3.2. Bond-splitting tests with large embedment length

Prismatic specimens were cast with a wire embedded longitudinally in the specimen. The dimensions of the prismatic specimens were 400 mm in length, 60 mm in width and with three different concrete covers. Figure 13 shows the geometry and dimensions of the specimens. The cross section of the specimens had the shape of a slender rectangle to obtain only two splitting cracks,

(a)

(b)

Figure 11. Two examples of splitting failure in precast prestressed joists.

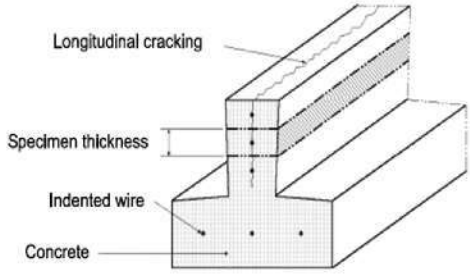

Figure 12. Sketch of a joist with a longitudinal splitting crack. The part selected for the study is indicated by a different weave.

perpendicular to the longer sides of the rectangle. Table V shows the specimen nomenclature and the concrete cover. The thinnest cover was adopted in accordance with the smallest distance between wires in a common prestressed joist or hollow core slab.

Before casting the concrete, the wires were tensioned to 17 kN in stiff vertical steel frames, between points A and B (see Figure 14). Then the concrete was cast. After hardening of the concrete, the prestressing force of the wire was transferred, under control, to the concrete prism, by moving the actuator upward at a rate of 0.3 mm/min. The gradual release of the wire (at point B) transferred the force to the concrete prism. The test ended when the free ends of the wire were

Table II. Composition of the concrete mixture.

Component	Quantity (kg/m^3)	Mixture proportion by weight
Cement	450	1.00
Water	225	0.50
Sand	900	2.00
Coarse aggregate	720	1.60

Table III. Mechanical properties of the materials.

Concrete	Steel wire
$E=38\,\text{GPa}$	$E=226\,\text{GPa}$
$f_c=57\,\text{MPa}$	$\sigma_{0.2}=1.755\,\text{MPa}$
$f_t=3.0\,\text{MPa}$	$\sigma_u=1.935\,\text{MPa}$
$G_F=100\,\text{N/m}$	$\varepsilon_u=5.25\%$

Table IV. Deepness of the wire indentation.

Denomination	Indentation depth (mm)
Shallow	0.01–0.02
Medium	0.04–0.06
Deep	0.1–0.11

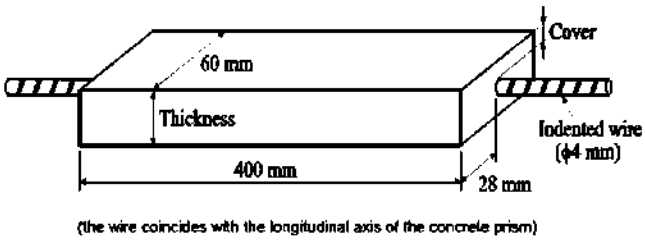

Figure 13. Geometry and dimensions of the *large* embedment length specimens.

Table V. Dimensions of the tested *large* embedment length specimens (see Figure 13).

Specimen	Thickness of specimen (mm)	Concrete cover (mm)
C1	14	5
C2	22	9
C3	30	13

completely unloaded. Figure 14 shows a sketch of the prestressing frame, with the specimen in the testing machine. During the tests the following parameters were recorded:

- Released load supplied by the testing machine.
- Displacement of the actuator of the testing machine.
- Longitudinal shortening of the concrete prism, measured with a gage length of 387.5 mm. Measurements were taken on opposite faces and the mean value was recorded.
- Wire-concrete slip on the upper and lower faces of the prismatic specimens.
- Crack opening displacement (COD) of the longitudinal cracks. Measurements were taken on opposite faces, those with the thinnest cover.

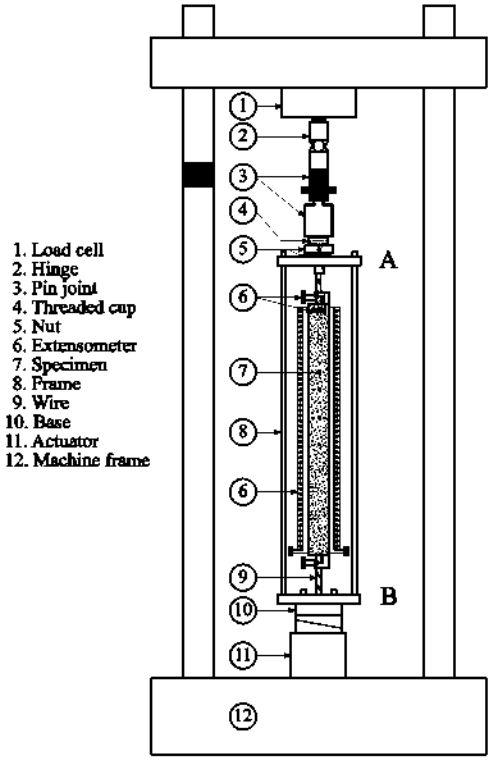

Figure 14. Sketch of the test setup for the *large* embedment length specimens.

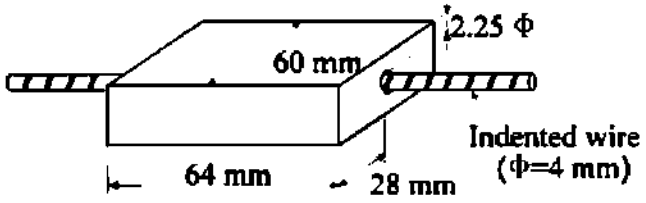

Figure 15. Geometry and dimensions of the *short* specimens.

For detailed information about specimen preparation, testing procedure and testing equipment, see [23, 25].

3.3. Bond-splitting tests with short embedment length

Similar prismatic specimens, as described above, were cast with a wire embedded longitudinally in the specimen. The dimensions of the prismatic specimens were 64 mm in length, 60 mm in width and 2.25 times the wire diameter concrete cover. The bonded length of the wire was 24 mm, placed in the central part of the specimen, with the bond between wire and concrete at the ends of the specimen being avoided. Figure 15 shows the geometry and dimensions of the specimens.

In the same way as the *large* specimens, before casting the concrete, the wires were tensioned to 17 kN in stiff vertical steel frames, between points A and B (see Figure 16). Then the concrete was cast. After hardening, the prestressing force was gradually released at A, causing the movement of the wire into the direction of B. As concrete is supported at C, the wire movement generated bond stresses between concrete and wire. Figure 17 shows a photo of the prestressing frame, with

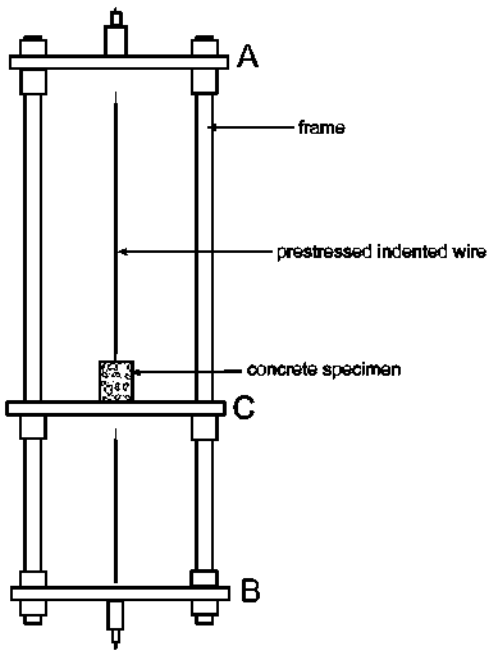

Figure 16. Sketch of the test setup for the *short* embedment length specimens.

the specimen in the testing machine. During the tests the following parameters were recorded:

- Released load supplied by the testing machine.
- Displacement of the actuator of the testing machine.
- Deformation of the wire between point A and C (upper part of wire).
- Deformation of the wire between point C and B (bottom part of wire).
- Wire–concrete slip on the upper faces of the prismatic specimens.
- COD of the longitudinal cracks. Measurements were taken on opposite faces, those with the thinnest cover.

To avoid the friction between the specimen and the plate support C a thin sheet of polytetrafluoridethylene (PTFE) was inserted. For detailed information about specimen preparation, testing procedure and testing equipment, see [26].

4. MODEL VALIDATION

4.1. Large embedment length specimen tests

The presented numerical model is used to reproduce the experimental results. Table III shows the mechanical properties of the materials, and Table VI the parameters adopted for the interface for the three depths of the indentations. These parameters were not experimentally measured, but estimated, based on previous tests [26]. The value of the u_{cd} (see Equation (11)) was the maximum indentation depth for each type of wire (see Table IV). Figure 18 shows a sketch of the finite element mesh. One quarter of the specimen was meshed due to its symmetry.

Figures 19(a)–(c) show the experimental records and the numerical prediction of the released load versus longitudinal shortening of the concrete prism, for specimens with shallow, medium and deep wire indentations, and the minimum concrete cover (5 mm). The recorded curves of the specimens with the thinnest concrete cover show a point where the slope of the curves markedly changes. Behind this point the longitudinal shortening of the concrete prism diminishes while the testing machine releases the tension of the wire. This special point marks the beginning of the

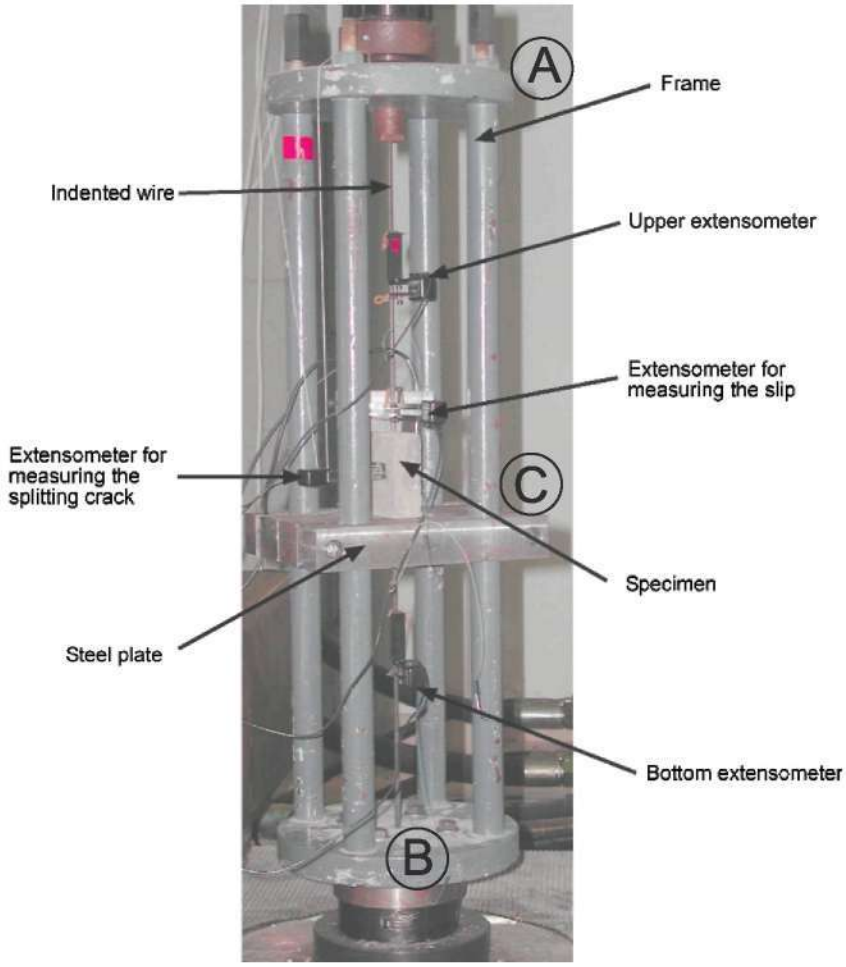

Figure 17. *Short* embedment length specimen during testing.

Table VI. Parameters of the interface adopted for numerical modelling of *large* embedment length specimens.

Denomination	τ_{max} (MPa)	σ_{t0} (MPa)	C_0 (MPa)	$\phi_d(^\circ)$	$\phi_f(^\circ)$
Shallow	10	3.0	8.4	0,3	40
Medium	10	3.0	8.3	4	42
Deep	10	3.0	8.2	16	43

longitudinal splitting of the concrete prism. The splitting cracks reduce the friction between the steel and concrete due to the loss of the wire confinement, and consequently induce a release of part of the compressive force in concrete, which diminishes the longitudinal shortening of the concrete prism, as seen in the experimental records. Specimens with 9 and 13 mm thickness concrete cover did not show splitting and were not used for the model validation.

Figure 20 shows the experimental records and the numerical prediction of the released load versus COD of the splitting crack, measured on the upper face of the specimen. Each curve shows a breakpoint corresponding to the opening of the crack, shown by a fast rise of the extensometer measurement. The breakpoint load coincides with that in Figures 19(a)–(c) and confirms the interpretation of those figures.

Figure 21 shows the experimental records and the numerical prediction of released load versus penetration of the wire into concrete, measured on the upper face of the specimens, for specimens

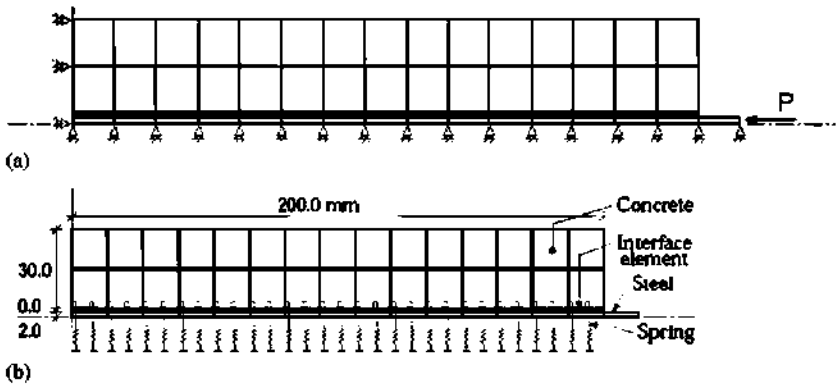

Figure 18. Sketch of the finite element mesh used for the numerical analysis of the *large* embedment length specimens: (a) boundary conditions and applied load and (b) materials and dimensions.

with medium and deep wire indentation, and cover of 5 mm. The specimens show a marked change in the slope of the curve. This point corresponds with the start of splitting and complements the above comments for these specimens. The splitting leads to a loss of confinement of the wire, increasing the slip between concrete and steel, with a greater penetration of the wire into concrete. Similar behaviour was observed in the specimens with shallow depth wire indentation, although specimens with shallow indentation showed a smoother change in the curves than ones with medium and deep indentation. Experimental curves of load versus penetration of the wire in the concrete, measured on the bottom face of the specimens, were practically equal to those of the upper face.

In all cases the numerical prediction properly predicts the bond behaviour and the coupled splitting failure. The prediction matches quite well the entire experimental records.

4.2. Short embedment length specimen tests

The results of two experimental tests were adopted for the model validation with the short embedment length specimens. One of the specimens had weakened bond, intentionally induced reducing the bond between wire and concrete. Both specimens showed splitting induced by the bond between wire and concrete.

Figure 22 shows the finite element mesh. A quarter of the specimen was meshed due to its symmetry. A 3D analysis was performed because of the short length of the specimen. Figure 22 shows three differentiated zones: concrete, bonded steel and unbonded steel. The unbonded steel has not been represented completely to diminish the computational cost, adopting an equivalent stiffness considering the complete length of the wire. The prestressing force was applied as a compression force at the top of the bonded steel. Table VII shows the interface parameters adopted for the finite element calculation. The 3D analysis is more accurate when taking into account the effects of the unbounded part of the steel, the sheet of PTFE on the bonded part of the steel, and the effect of the short length of the specimen.

The influence of the mesh size has been also studied. Figure 23 shows two finite element meshes, fine and coarse, adopted to study a possible mesh-size dependence on the results.

Figure 24 shows the experimental records and the numerical prediction of the released force versus the bond stress for both specimens. The specimen with the weakened bond shows lower tangential stress and slope of the curve. Figure 25 shows the experimental records and the numerical prediction of the released force versus the slip between wire and concrete for both specimens. No mesh-size dependence is appreciated.

In both cases the numerical prediction properly predicts the bond-slip experimental behaviour and the coupled splitting failure. The splitting process is shown by the plateau of the curve in Figure 24 for the specimen with good bond, after a value of the released load of 11 kN. As the

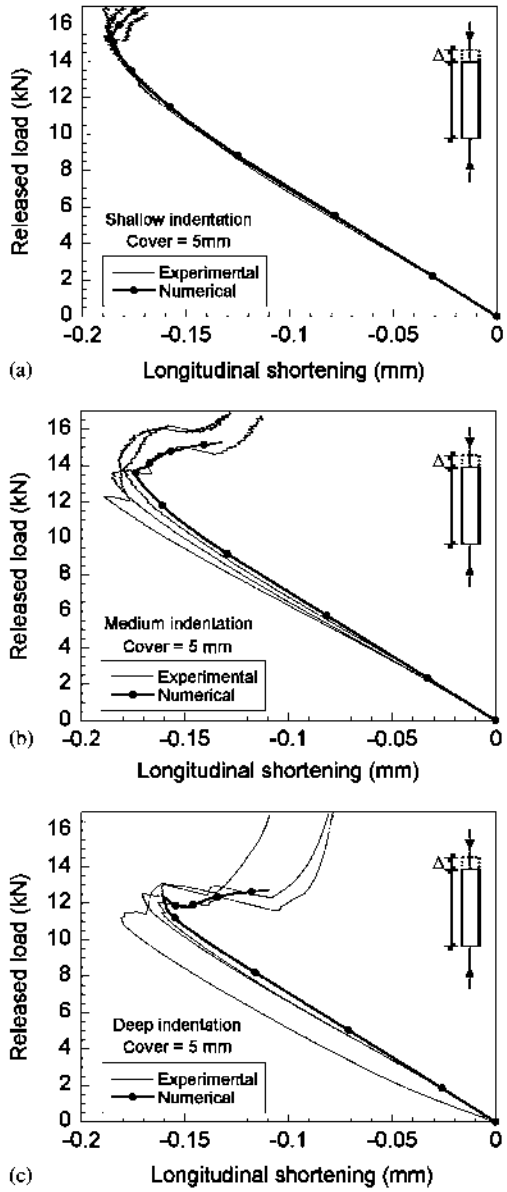

Figure 19. Experimental records and numerical prediction of released load versus longitudinal shortening of the concrete prism in *large* embedment length specimens with 5 mm of thickness concrete cover and wire indentation: (a) shallow; (b) medium; and (c) deep.

dilatancy angle is very low on the simulation of the behaviour of the specimen with weakened bond, the splitting action is practically undetectable.

To avoid the friction between concrete and steel plate, different frictionless materials may be used (in the experimental work PTFE was adopted). The relative stiffness between concrete and frictionless material sheet influences the released load versus the bond stress curve (see Figure 26(a)) and the released load versus slip between concrete and wire curve (see Figure 26(b)). This aspect influences the splitting action of the bond in the tested specimens. The numerical model may be useful to study this particular aspect. Figure 26 shows both numerical predictions for a sheet of frictionless material of 0.1 mm of thickness and Young's modulus of 10^9, 100 and 3 MPa, respectively. The lowest stiffness frictional sheet generates the highest influence on the bond between wire and concrete. There is no significant difference between rigid and semi-rigid sheet, for the thickness of the sheet studied.

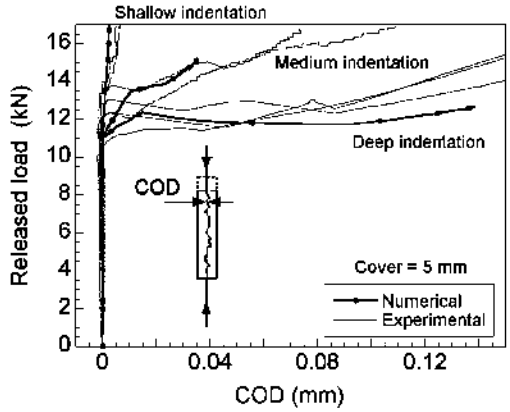

Figure 20. Experimental records and numerical prediction of released load versus COD of the splitting crack of the concrete prism in *large* embedment length specimens with 5 mm of thickness concrete cover and three depths of the wire indentation.

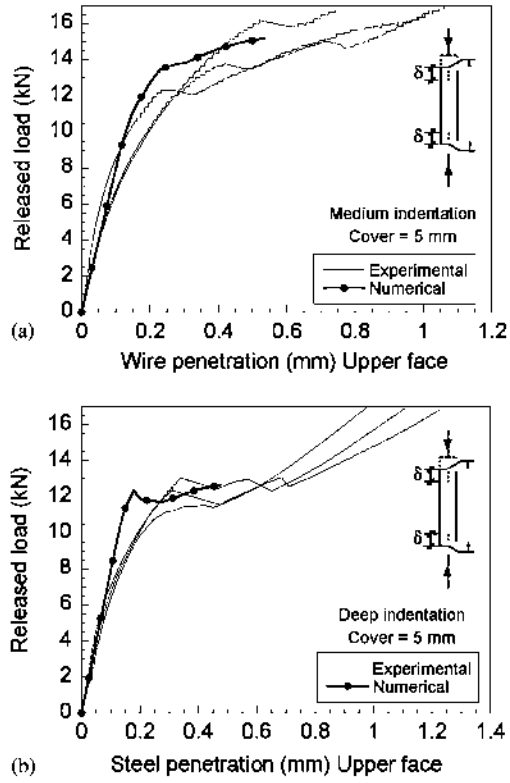

Figure 21. Experimental records and numerical prediction of released load versus wire penetration into concrete prism in *large* embedment length specimens with 5 mm of thickness concrete cover and deepness of the wire indentation: (a) medium and (b) deep.

5. DISCUSSION

The above proposed model accurately reproduces the experimental records, for large and short embedment length specimens. The model improves the previous proposals [17–19] for ribbed steel bars and includes the splitting action of the bond by means of a coupled cohesive fracture model for concrete. The model relates average local slip, radial dilatation, bond shear stress and radial

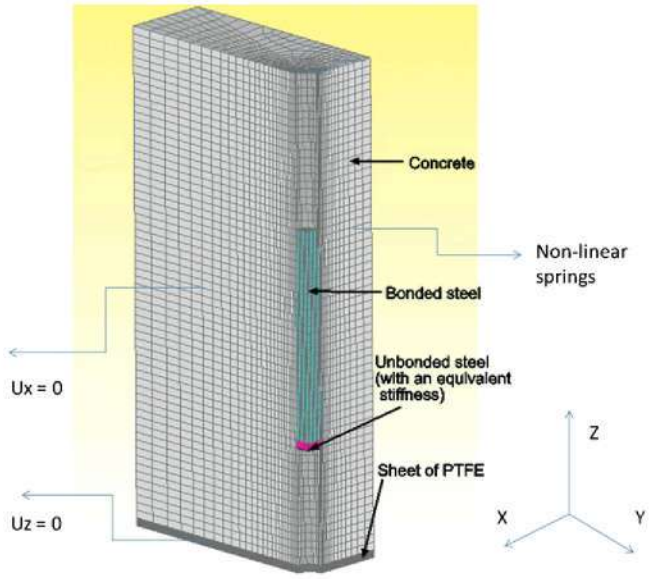

Figure 22. Finite element mesh for *short* embedment length specimens.

Table VII. Parameters of the interface adopted for numerical modelling of *short* embedment length specimens.

Specimen	σ_{t0} (MPa)	C_0 (MPa)	$\phi_d(^\circ)$	$\phi_f(^\circ)$
Good bond	3.2	2.5	0.25	20
Weakened bond	0.3	0.2	2×10^{-2}	20

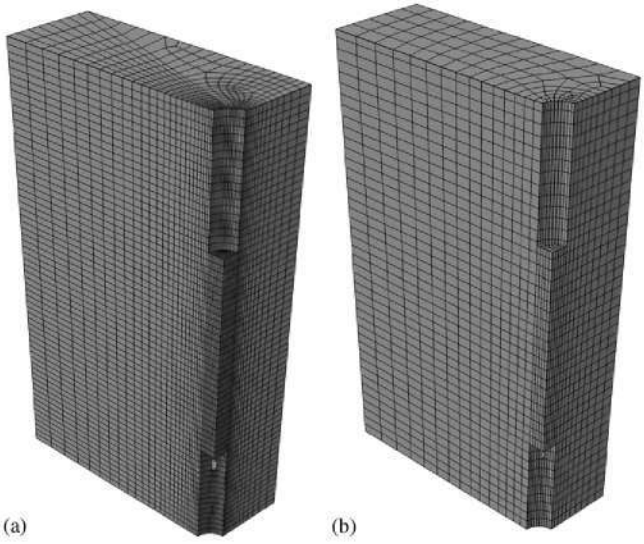

Figure 23. Finite element mesh for *short* embedment length specimens: (a) fine mesh and (b) coarse mesh.

confinement stress to splitting of the concrete. The model has been developed for indented wires and takes into account the influence of the depth indentation. Extension of the model to strands by adopting the suitable parameters does not present significant problems, especially with regard to the equivalent perimeter in contact with concrete.

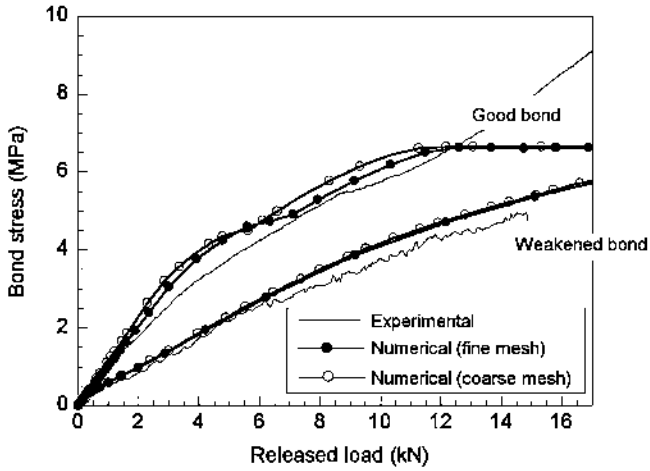

Figure 24. Experimental records and numerical prediction of released load versus bond stress in *short* embedment length specimens with good and weakened bond between wire and concrete.

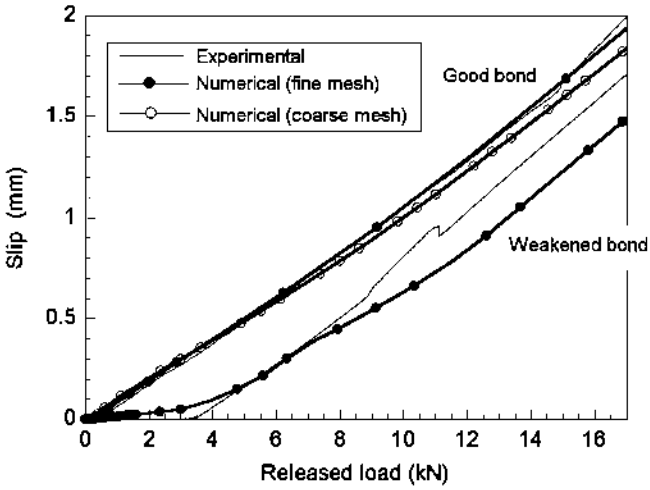

Figure 25. Experimental records and numerical prediction of released load versus bond slip in *short* embedment length specimens with good aud weakened bond betweeu wire and concrete.

The mechanical properties of the concrete and steel (Table III) and the depth of the wire indentation (Table IV) have been previously measured to the numerical simulation. The parameters of the interface, Table VI for large embedment length specimens and Table VII for short length specimens, have been estimated, based on previous tests [26]. All these parameters are required data for the numerical procedure, and should be previously known. The experimental records of the released load versus longitudinal shortening (Figure 19), versus COD (Figure 20) and versus steel penetration (Figure 21) of the large embedment length specimens have been used for validation. The analogous experimental records of the short embedment length specimens have been also used for validation: the released load versus bond stress (Figure 23) and slip (Figure 24).

The differences between bond model parameters shown by Tables VI and VII are explained by the differences of behaviour between short and large embedment lengths of the wire in the concrete specimens. On short specimens the influence of local mechanical interaction of indentation with the adjacent concrete is very important. The length (3.5 mm) and spacing (5.5 mm) of the indentation are significantly high in comparison with the bonded length (24 mm). These local effects are not so important in the large length embedment specimens, which average them along the large length.

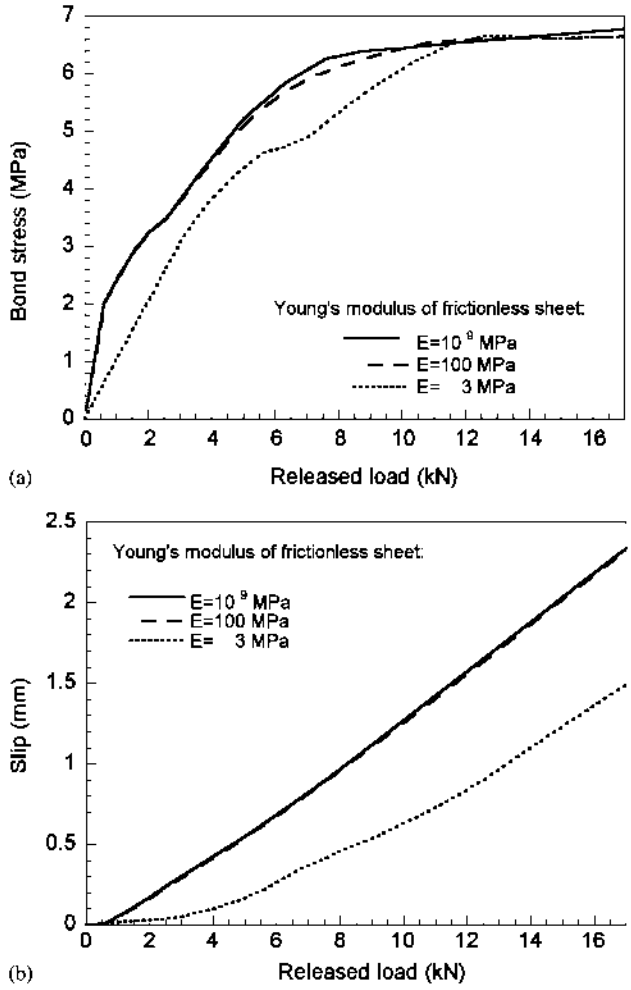

Figure 26. Influence of the Young's modulus of the frictionless sheet on the *short* embedment length specimen bond-splitting tests: (a) released load versus bond stress and (b) released load versus slip between wire and concrete.

Large length embedment specimens average in a more consistent form the local effects than short length specimens. 'Indentation-scale' analysis of the cracking and crushing of concrete adjacent to wire will be welcomed. This paper deals with 'wire-scale', according to Cox and Hermann [18, 19] terminology.

As only the specimens with the thinnest concrete cover exhibited splitting induced by bond, only they were adopted for the numerical validation. The smallest thickness of the concrete cover, 5 mm (1.25 times the wire diameter), is apparently much thinner, but is based on the real dimensions used by the industry for certain precast prestressed joists (see Figures 11 and 12).

The comparison of the experimental records and numerical simulation of the released load versus specimen shortening, COD and wire penetration has shown the deepest indentation and the highest splitting action of the wire.

As regards the experimental work, the specimens were designed to guarantee that the splitting crack grew in a fixed direction, perpendicular to the largest face of the specimen in the cross section (see Figures 12 and 13). This design facilitates the detection of the splitting of the concrete and the measurement of the COD. There was not any need to use localization algorithms for the numerical procedure, and a cohesive crack model inserted in the crack path was enough for the numerical splitting simulation. This simple procedure facilitates analysis of the influence of the parameters affecting bond in the splitting failure of the concrete.

The discrete cohesive crack approach is successful when there is one crack on the concrete [28], although other cracking models may be adopted, such as damage models or smeared crack models.

6. CONCLUSIONS AND FINAL COMMENTS

A numerical procedure for modelling the bond-slip at the interface of the wire and concrete has been proposed. The procedure takes into account the possible failure of concrete by the splitting action of the wire. The bond modelling is based on a non-associative plasticity approach, and the splitting concrete modelling on the cohesive crack approach for quasi-brittle materials.

The bond model was incorporated into an interface finite element. The cohesive crack model for the simulation of the radial cracks was included by means of non-linear springs. Both models were incorporated in the finite element code ABAQUS©. The numerical procedure has been contrasted with two series of experimental results, and accurately reproduces the experimental records.

Splitting failure induced by bond is adequately reproduced by the numerical model. The failure is observed by means of a change in the slope of the released load versus longitudinal shortening curves. The longitudinal shortening of the specimen decreased after splitting failure, indicating the loss of wire confinement. The critical released load that showed the splitting failure diminished when the depth of the wire indentations increased.

The COD measurement simulation has enabled detection and monitoring of the splitting failure to be carried out more easily. Moreover, the deepest depth wire indentation the earliest (load released) and largest COD in the longitudinal cracking failure.

The greatest depth wire indentation leads to the best bond between wire and concrete, until the splitting failure. This better behaviour is shown by a lower sliding of the wire at the end of the specimen and by a larger longitudinal shortening of the specimen for equal released load in the recorded experimental curves. It is worth noting that the deeper wire indentation leads to a higher splitting stresses and to a larger COD in the specimens.

The numerical procedure emphasizes that the cohesive crack models, in combination with the bond modelling, are promising tools in the simulation of the splitting failure of the precast prestressed concrete structural elements. Further work must be carried out to extend this modelling to full-scale structural elements.

ACKNOWLEDGEMENTS

The authors gratefully acknowledge the fiuancial support for the research provided by the Spanish Ministerio de Ciencia e Innovación under grant BIA-2008-03523 and by the Ministerio de Fomento under grant MFOM-01/07.

REFERENCES

1. Tepfers R. A theory of bond applied to overlapped tensile reinforcement slices for deformed bars. Chalmers University of Technology, Division of Concrete Structures, Götegorg, Sweden, 1973; publication 73:2.
2. Tepfers R, Olsson PÅ. Ring test for evaluation of bond properties of reinforcing bars. *Bond in Concrete: From Research to Practice*, vol. 1. Riga Technical University and CEB: Latvia, Riga, 1992; 89–99.
3. Cairns J, Jones K. The splitting forces generated by bond. *Magazine of Concrete Research* 1995; **47**:153–165.
4. Cairns J, Jones K. An evaluation of the bond-splitting action of ribbed bars. *ACI Materials Journal* 1996; **93**:10–19.
5. Gambarova PG, Rosati GP. Bond and splitting in reinforced concrete: test results on bar pull-out. *Materials and Structures* 1996; **29**:267–276.
6. Abrishami H, Mitchell D. Simulation of uniform bond stress. *ACI Materials Journal* 1992; **89**(2):161–168.
7. Ogura N, Bolander JE, Ichinose T. Analysis of bond splitting failure of deformed bars within structural concrete. *Engineering Structures* 2008; **30**(2):428–435.
8. Jendele L, Cervenka J. Finite element modeling of reinforcement with bond. *Computers and Structures* 2006; **84**(28):1780–1791.
9. Malvar J. Bond of reinforcement under controlled confinement. *ACI Materials Journal* 1993; **89**:593–601.

10. den Uijl JA. Bond and splitting action of prestressed strand. *Bond in Concrete: From Research to Practice*, vol. 2. Riga Technical University and CEB: Latvia, Riga, 1992; 79–88.
11. Abrishami H, Mitchell D. Bond characteristics of pretensioned strand. *ACI Materials Journal* 1993; **90**(3):228–235.
12. Tassios T, Bonataki E. Experimental analysis of the bond behaviour of prestressed tendons. *Bond in Concrete: From Research to Practice*, vol. 2. Riga Technical University and CEB: Latvia, Riga, 1992; 29–37.
13. FIB 2000. Bond of reinforcement in concrete. State-of-art report task group bond models. *FIB Bulletin*, 2000; 10.
14. Noghabai K. Discrete versus smeared versus element-embedded crack models on ring problems. *Journal of Engineering Mechanics* 1999; **125**(3):307–315.
15. den Uijl JA, Bigaj AJ. A bond model for ribbed bars based on concrete confinement. *HERON* 1996; **41**(3):201–226.
16. van der Veen C. Splitting failure of reinforced concrete at various temperatures. In *Fracture Processes in Concrete Rock and Ceramics*, van Mier JGM, Rots JG, Baker A (eds). RILEM: London, 1991.
17. Cox JV. Development of a plasticity bond model for reinforced concrete—Theory and validation for monotonic applications. *TR-2036-SHR*, Naval Facilities Engineering Service, Port Hueme, CA, 1994.
18. Cox JV, Hermann R. Development of a plasticity bond model for steel reinforcement. *Mechanics of Cohesive-Frictional Materials* 1998; **3**:155–180.
19. Cox JV, Hermann R. Validation of a plasticity bond model for steel reinforcement. *Mechanics of Cohesive-Frictional Materials* 1999; **4**:361–389.
20. Janney JR. Nature of bond in pretensioned prestressed concrete. *ACI Journal* 1954; **25**(8):717–736.
21. Gustavson R. Experimental studies of the bond response of three-wire strands and some influencing parameters. *Materials and Structures* 2004; **37**:96–106.
22. UNE 36094. *Steel Wires and Strands for Prestressing Concrete*. AENOR: Madrid, Spain, 1997.
23. Gálvez JC, Tork B, Planas J. Concrete splitting during the release of prestressing force in indented wires. In *Bond in Concrete*, Balázs G, Bartos P, Cairns J, Borosnyói A (eds). Budapest University of Technology and Economics: Budapest, 2002; 95–102.
24. Gambarova PG, Rosati GP, Zasso B. Steel-to-concrete bond after concrete splitting: constitutive laws and interface deterioration. *Materials and Structures* 1989; **22**(131):347–356.
25. Tork B. Study of the bond-splitting combined mechanisms in reinforced and prestressed concrete elements (in Spanish). *Ph.D. Thesis*, University of Politécnica, Madrid, 1999.
26. Benítez JM. Study of the interaction between presstresed wire and concrete during release of the prestressing force (in Spanish). *Ph.D. Thesis*, University of Castilla La Mancha, 2006.
27. Hillerborg A, Modeer M, Petersson P. Analysis of crack formation and crack growth in concrete by means of fracture mechanics and finite elements. *Cement and Concrete Research* 1976; **6**:773–782.
28. Bažant ZP, Planas J. *Fracture sand Size Effect in Concrete and Other Quasibrittle Materials*. CRC Press: New York, 1998.
29. ASTM C/C498-04e1. *Standard Test Method for Splitting Tensile Strength of Cylindrical Concrete Specimens*. ASTM International: West Conshohocken, PA, 2004.
30. RILEM 50-FMC Committee Fracture Mechanics of Concrete. Determination of the fracture energy of mortar and concrete by means of three-point bend tests on notched beams. *Materiaux et Constructions* 1986; **18**:285–290.
31. Gálvez JC, Cervenka J, Saouma V, Cendón DA. A discrete crack approach to normal/shear cracking of concrete. *Cement and Concrete Research* 2002; **32**:1567–1585.
32. Gálvez JC, Cendon DA, Planas J. Influence of shear parameters on mixed-mode fracture of concrete. *International Journal of Fracture* 2002; **118**:163–189.
33. Cervenka J. Discrete crack modelling in concrete structures. *Ph.D. Thesis*, University of Colorado, 1994.
34. prEN 10138-2. *Prestressing Steels—Part 2: Wire*. European Committee for Standardization: Brussels, 2000.